Formation and maintenance of nitrogen-fixing cell patterns in filamentous cyanobacteria

Javier Muñoz-García[a] and Saúl Ares[a,1]

[a]Grupo Interdisciplinar de Sistemas Complejos (GISC) and Departamento de Matemáticas, Universidad Carlos III de Madrid, 28911 Leganes, Spain

Edited by Robert Haselkorn, University of Chicago, Chicago, IL, and approved April 7, 2016 (received for review December 10, 2015)

Cyanobacteria forming one-dimensional filaments are paradigmatic model organisms of the transition between unicellular and multicellular living forms. Under nitrogen-limiting conditions, in filaments of the genus *Anabaena*, some cells differentiate into heterocysts, which lose the possibility to divide but are able to fix environmental nitrogen for the colony. These heterocysts form a quasiregular pattern in the filament, representing a prototype of patterning and morphogenesis in prokaryotes. Recent years have seen advances in the identification of the molecular mechanism regulating this pattern. We use these data to build a theory on heterocyst pattern formation, for which both genetic regulation and the effects of cell division and filament growth are key components. The theory is based on the interplay of three generic mechanisms: local autoactivation, early long-range inhibition, and late long-range inhibition. These mechanisms can be identified with the dynamics of *hetR*, *patS*, and *hetN* expression. Our theory reproduces quantitatively the experimental dynamics of pattern formation and maintenance for wild type and mutants. We find that *hetN* alone is not enough to play the role as the late inhibitory mechanism: a second mechanism, hypothetically the products of nitrogen fixation supplied by heterocysts, must also play a role in late long-range inhibition. The preponderance of even intervals between heterocysts arises naturally as a result of the interplay between the timescales of genetic regulation and cell division. We also find that a purely stochastic initiation of the pattern, without a two-stage process, is enough to reproduce experimental observations.

cyanobacteria | pattern formation | activator–inhibitor | heterocyst differentiation | gene-regulatory networks

Cyanobacteria were pioneer organisms to use oxygenic photosynthesis and are currently one of the most successful living groups, occupying a broad range of habitats across all latitudes and producing a large fraction of Earth's photosynthetic activity. Some types of cyanobacteria form colonies consisting of one-dimensional filaments of vegetative cells carrying photosynthesis. However, as a response to different environmental stresses, vegetative cells can differentiate into specialized cell types that perform important functions for the survival of the colony. This is a paradigmatic example of a prokaryotic form of life with differentiated cell types.

Bacteria and archaea are the only forms of life able to fix atmospheric nitrogen, making them crucial for all living forms on Earth. N_2 fixation is catalyzed by nitrogenase, and this enzyme is easily degraded by oxygen. Some filamentous cyanobacteria have developed a mechanism to protect nitrogenase from the oxygen produced by vegetative cells. When external nitrogen sources are scarce, specialized cells called heterocysts appear in a quasiregular pattern, with intervals of around 10 vegetative cells between consecutive heterocysts. Because cells can exchange metabolites and small peptides (1–6), the fixed nitrogen produced by heterocysts can reach vegetative cells. N_2 fixation requires high energy consumption. To maintain it, nutrients produced by photosynthesis in vegetative cells are shared with heterocysts (4, 7). Upon differentiation, heterocysts lose the possibility to undergo cell division. However, vegetative cells continue dividing, producing filament growth and increasing the distance between consecutive heterocysts. As a result, new heterocysts differentiate roughly in the middle of the intervals between previously existing heterocysts. This dynamic process of differentiation allows the overall pattern to conserve its properties over time.

The biology of heterocyst formation has been the subject of intensive work (4, 8). Most studies focus on the strain PCC 7120 of the genus *Anabaena*, which has become a model organism in the field. Recent quantitative experimental work has produced a wealth of data on vegetative cell intervals between heterocysts under a number of mutations and experimental conditions. Moreover, the one-dimensional nature of this pattern-forming system represents a very appealing system for theoretical and mathematical modeling (9–20).

Despite these efforts, many processes and genetic mechanisms involved in the regulation of heterocyst differentiation, pattern formation, and maintenance remain poorly understood. For example, it has not been clarified which particular vegetative cells differentiate into heterocysts and if this is related to some inherited predisposition (21, 22). Other open questions are whether the differentiating cells are selected stochastically, how the typical spacing between heterocysts is determined for cells differentiating at early and late times, or which mechanisms induce the appearance of multiple contiguous heterocysts, the so-called Mch phenotype (23), in some mutants.

Basic Genetics of Heterocyst Differentiation

There is a large number of processes involved in the regulation of heterocyst pattern formation. In addition to nitrogen levels and other environmental aspects, many genes and factors play a role (24). When nitrogen stress is perceived, the transcriptional regulator *ntcA* is important to trigger heterocyst differentiation (25, 26), directly or indirectly controlling the expression of several genes (27, 28), including *hetR*. The gene *hetR* is central to heterocyst differentiation. Its expression is the main positive regulatory factor in heterocyst development (29–32). The expressions

Significance

Cyanobacteria produce an important fraction of oxygen on Earth and, together with archaea, fix atmospheric nitrogen used by all other organisms. Some types live in colonies with specialized cells that perform different functions. In particular, the genus *Anabaena* forms filaments in which some cells differentiate, forming patterns to effectively provide nitrogen for the colony. We present a theory that combines genetic, metabolic, and morphological aspects to understand this prokaryotic example of multicellularity. Our results quantitatively reproduce the appearance and dynamics of this pattern and are used to learn how different aspects, like fixed-nitrogen diffusion, cell division, or stochasticity, affect it.

Author contributions: J.M.-G. and S.A. designed research, performed research, and wrote the paper.

The authors declare no conflict of interest.

This article is a PNAS Direct Submission.

[1]To whom correspondence should be addressed. Email: saul@math.uc3m.es.

This article contains supporting information online at www.pnas.org/lookup/suppl/doi:10.1073/pnas.1524383113/-/DCSupplemental.

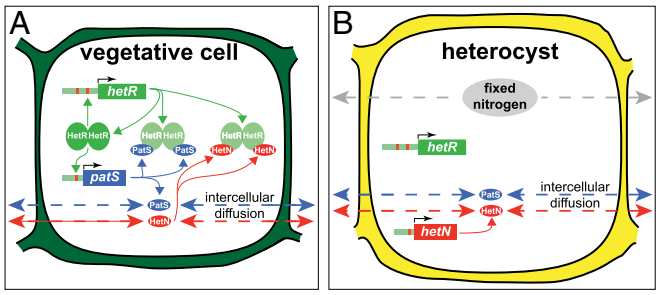

Fig. 1. Minimal model of the genetic network. (*A*) In vegetative cells, HetR dimers can activate the expression of *hetR* and *patS*. (*B*) In heterocysts, *hetN* is expressed constitutively and fixed-nitrogen products are produced. Active products of PatS and HetN, possibly the RGSGR pentapeptide, can diffuse between cells of any kind in the filament and bind HetR, preventing it from binding DNA. Fixed-nitrogen products also diffuse to other cells and contribute weakly to inhibit differentiation.

of *ntcA* and *hetR* are mutually dependent, and the latter seems to be necessary and sufficient for heterocyst development, even under conditions of excess of external nitrogen (33). Thus, positive autoregulation of *hetR* is required for differentiation and is particularly significant in developing heterocysts (30, 34). In addition to *ntcA*, other genes such as *patA*, *hetF*, and *hetP* also regulate heterocyst differentiation (35–38).

The gene *patS* is a negative regulator of *hetR* that suppresses differentiation when overexpressed and induces a Mch phenotype when deleted (23, 39, 40). PatS is a short peptide, predicted to be 13 or 17 aa, containing a carboxyl-terminal pentapeptide RGSGR that prevents DNA binding activity of HetR (41, 42) and inhibits differentiation when added to culture medium (23). The expression of *patS* in small groups of vegetative cells was shown to diminish the levels of HetR in adjacent cells (43), suggesting that a PatS-dependent signal can diffuse along the filament (44). It has been observed that *patS* is strongly expressed in developing heterocysts (23, 39), coming back to low levels after 24 h of nitrogen deprivation. Although lack of *patS* expression initially produces a pattern with frequent contiguous heterocysts and short intervals between separate ones, later this pattern tends to become more similar to a wild-type pattern (39), suggesting the presence of other patterning signals.

Thus, *hetR* and *patS* could be enough to obtain a minimalistic understanding of heterocyst pattern formation at early stages. However, other players have to be taken into account to explain pattern maintenance after an initial pattern of differentiated heterocysts appear. The key player for this role is the inhibitory factor *hetN*. Akin to PatS, HetN also contains a RGSGR motif, raising the possibility that a RGSGR-containing peptide derived from the full protein diffuses from cell to cell (45). In contrast to *patS* mutants, *hetN* mutants have a differentiation pattern similar to the wild type at the initial stages of nitrogen depletion and a Mch phenotype after 48 h (46), suggesting that *hetN* expression is activated later than that of *patS*. When both genes are suppressed, almost all cells along the filament eventually differentiate, causing lethal levels of heterocysts (47).

Metabolites have also been suggested to play a role in filament patterning, in particular the fixed-nitrogen products produced by heterocysts. It has been suggested that they inhibit heterocyst differentiation (39), although experiments with *Anabaena variabilis* (48, 49) did not find an observable effect.

Results

Minimal Model for the Heterocyst Differentiation Gene-Regulatory Network. Although the chemical and genetic regulation of heterocyst differentiation involves a great number of factors (4, 8, 24), we will focus on the core mechanisms involved: local autoactivation, early long-range inhibition, and late long-range inhibition. For concreteness, we will identify these generic mechanisms with the dynamics of three genes: *hetR*, *patS*, and *hetN*, and use what is known of their biochemistry to build a theoretical model. To first approximation, the effects of other genes like *ntcA* or *patA* could be included in a phenomenological way, as factors affecting the parameters. This approach will not capture all of the subtleties that the explicit inclusion of all possible effects would produce, but has the advantage of being generic, clear, and simple, allowing a more systematic analysis of the model.

Fig. 1 shows a diagram of the minimal genetic network considered in our theoretical description. Upon nitrogen deprivation, *hetR* is expressed, partly in a constitutive way (34). Its protein acts as a dimer (42, 50, 51), binding the *hetR* and *patS* promoter regions and activating expression. HetR has recently been observed also as a tetramer (52); including that information in our model would only change parameter values but not the dynamics of differentiation. A PatS product, the RGSGR pentapeptide, can bind HetR with a 1:1 stoichiometry, and RGSGR-tagged HetR molecules can no longer bind DNA (41, 53). Because HetN also contains the RGSGR motif, we assume that it binds and affects HetR analogously to PatS. PatS is only produced in vegetative cells, whereas HetN is exclusively produced in heterocysts. Because expression of HetR remains high in heterocysts (54), we model it through constitutive expression. We will show later that a second late inhibitor with fast diffusion and a weaker inhibition power than HetN is required to reproduce some experimental findings. A likely candidate for this inhibitor could be the effect of fixed-nitrogen products. Finally, we include intercellular diffusion of PatS, HetN, and fixed-nitrogen products. For simplicity, we do not represent RGSGR explicitly in our model, making instead its effect proportional to the concentration of PatS or HetN. Vegetative cells that maintain a threshold level of HetR during a predefined period are switched to heterocyst status.

In contrast to static patterns that are permanently defined once formed, the heterocyst pattern is a dynamic one: vegetative cells keep on growing and dividing, causing the intervals between contiguous heterocysts to continuously increase in size, until eventually a cell of the interval differentiates into a new heterocyst. Thus, we have included cell growth and division as a key ingredient of this model. Moreover, the stochastic nature of gene expression cannot be ignored, and especially the noise in the duration of the cell cycle can play a relevant role in defining the statistics of vegetative intervals between contiguous heterocysts. For this reason, noise should be included in a theoretical description, both in the genetic network and in cell division. The details of the mathematical formulation, analysis, and computer simulation of our model are described in *Supporting Information*.

From a physical perspective, the local (nondiffusive) character of the activator, the distinction between inhibitors acting at different times, and the dynamic character of the growing filament, are the features that set this problem apart from other reaction–diffusion pattern-forming systems.

The Theoretical Model Quantitatively Reproduces Wild-Type Patterns. A first feel of the properties of our model can be obtained by visual inspection of the patterns it produces (Fig. 2, Fig. S1, and

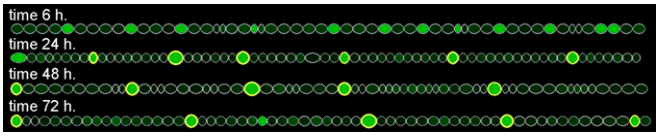

Fig. 2. Temporal evolution of a filament for the wild type. Heterocyst cells have a yellow membrane. The intensity of the green color shows the level of HetR concentration. Length of the cells represents its value in the simulation. See also Fig. S1 and Movie S1.

APPLIED MATHEMATICS

DEVELOPMENTAL BIOLOGY

Movie S1). Cells with high levels of HetR appear early (55), frequently in clusters. Eventually only some isolated cells differentiate into heterocysts, whereas the others revert to a low HetR state. Once a heterocyst pattern is established, cell division increases the vegetative interval length between heterocysts. At some point, one or a few cells roughly in the middle of the interval increase their HetR levels, and, finally, just one vegetative cell differentiates into a new heterocyst, thus maintaining the quasiregularity of the pattern.

The properties of heterocyst patterns can be quantified making a histogram showing the relative frequency of vegetative intervals of each length. Changes in the shape of this histogram allow to characterize differences between different phenotypes, and also between different stages of filament growth after nitrogen deprivation. We have obtained these histograms and other statistical data averaging over 192 different filaments of 150 initial vegetative cells. The histograms in Fig. 3 are remarkably similar to experimental ones (23, 39, 43, 44, 47, 56–60), reproducing details such as the increase of the typical length of vegetative intervals with time, the gradual broadening of the shortest intervals observed on the filament, or the higher frequency of even intervals. The analysis can be pushed further from qualitative observation to quantitative characterization. This can be done using successive moments of the distributions given by the histograms: mean, variance, and skewness. The mean gives an estimation of the average interval length, and the variance, of the width of the intervals distribution. The skewness is a measure of the asymmetry of the distribution. Positive skewness indicates that the right tail of the distribution is heavier than the left tail, which is the situation generally found in experiments. We have compared the temporal evolution of these magnitudes in our simulations together with equivalent statistics extracted from experimental histograms in the literature (Fig. 4). A first observation for the wild type is that the mean interval length slightly increases from 10 cells at 24 h up to 12 cells after a few days.

In the following, we proceed to discuss other conditions. To start with, in experiments, all cells of *hetR* mutants remain in the vegetative state (61). In the same way, because HetR is necessary for differentiation in our model, no heterocysts form in that condition. The same is true for any double knockdown involving *hetR*. Overexpression of *hetR* induces differentiation of all of the cells in the filament.

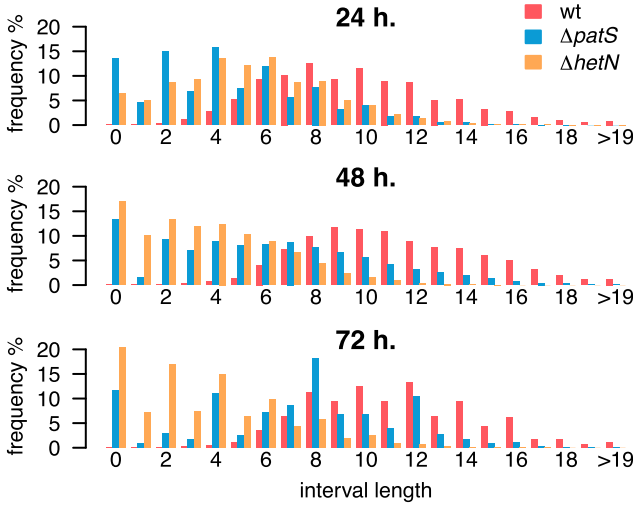

Fig. 3. Histograms of the number of vegetative cells between heterocysts. Conditions and times after nitrogen deprivation as indicated.

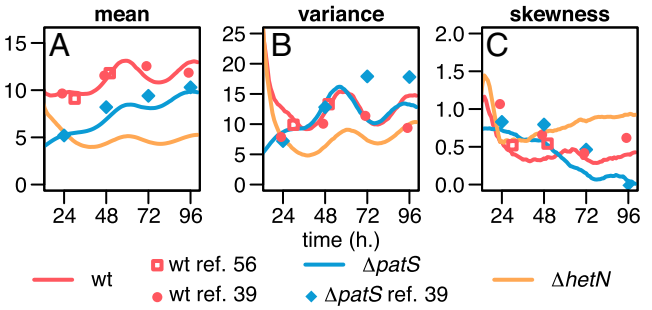

Fig. 4. Dynamics of heterocyst patterning. Time evolution of the (*A*) mean, (*B*) variance, and (*C*) skewness of the interval length distribution for our model (lines) and experimental results (symbols), as indicated. See Fig. S4*A* for a comparison of theory and experimental data on *hetN* loss of function.

PatS Promotes Early Pattern Formation. The early behavior of the *patS* mutant is quite different from the wild type (Fig. 5, Fig. S2, and Movie S2). Due to the lack of PatS, before differentiation there is no sequestration of HetR that can weaken its autoinducing feedback loop, so all cells build up high levels of HetR at short times. The first cells to differentiate start producing HetN that diffuses to their neighbors and prevents others from differentiating; however, an abnormally high number of cells, some of them contiguous, have already become heterocysts. This is the Mch phenotype observed in experiments (8, 23, 39, 47, 61). This high number of heterocysts inhibit differentiation until the vegetative interval between them becomes large enough. For this reason, at long times the Mch phenotype is attenuated and the pattern becomes more similar to wild type. Because new cells cannot appear between contiguous heterocysts, this phenotype persists as a hallmark of the irregular initiation of pattern formation in *patS* mutants. The histograms for the *patS* mutant (Fig. 3) show the predominance of contiguous heterocysts and short intervals at early times. Starting from mean intervals of five cells at 24 h, the mean converges to values similar to wild type after 4 d, as in experiments (Fig. 4*A*).

These results confirm that PatS is essential during the first stages of pattern induction to produce a regular pattern. At late stages, a regular pattern can be maintained even in the absence of PatS, pointing to the need of a subsequent inhibitor key for pattern maintenance. Continuing the study of the effect of PatS on filament development, we have also simulated PatS overexpression. As observed in experiments (23), we found a complete repression of heterocyst differentiation in the filament.

HetN Is Necessary, but Not Sufficient, for Pattern Maintenance: A Second Inhibitor, Probably Fixed-Nitrogen Products, Also Plays a Role. In the case of *hetN* loss of function, the presence of PatS assures a correct pattern formation until a first generation of heterocysts differentiates (Fig. 6, Fig. S3, and Movie S3). PatS produced in protoheterocysts inhibits the *hetR* feedback loop, but once those protoheterocysts differentiate into heterocysts, they cannot inhibit differentiation in their neighbors because they do not produce HetN. If the only mechanism of late long-range inhibition in the model is the *hetN* gene, in its absence, once a first pattern is established more and more cells continue to differentiate, until eventually the filament is almost entirely composed of heterocysts (Fig. S4*A* and Movie S4). This is far from experimental observations, where the loss of *hetN* condition does induce an increase in the number of heterocysts and a Mch phenotype that eventually stabilizes with time, forming a pattern with roughly 20% of heterocysts (46, 47, 61–63). This hints that a second late long-range inhibition mechanism must be at play to avoid the fatal differentiation of the whole filament. A natural candidate is the

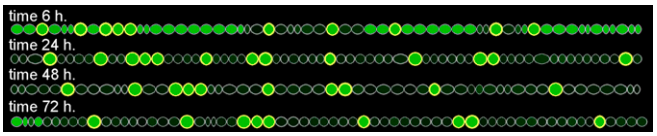

Fig. 5. Temporal evolution of a filament for the *patS* mutant. Details as in Fig. 2. See also Fig. S2 and Movie S2.

effect of fixed-nitrogen products produced by heterocysts (8, 39), although in principle it could be some other genetic or metabolic species. We have included it in our model explicitly, using a mechanism similar to that of HetN but with weaker inhibition power and larger diffusivity, which accounts for the smaller molecules involved (a detailed theoretical description of the effect of fixed nitrogen can be found in ref. 19). When the inhibition by fixed-nitrogen products is taken into account, the model reproduces quantitatively the experimental data from *hetN* loss of function (Fig. S4*A*). This suggests that, in a *hetN* loss-of-function background, fixed nitrogen plays a nonnegligible role in the maintenance of the pattern, a question that has been difficult to assess experimentally (8, 49). HetN and fixed-nitrogen products are not required for the appearance of the pattern but are essential for its maintenance at late stages. Because *hetN* is a much stronger inhibitor in our model, filaments in which fixed-nitrogen products have no function are identical to wild type (Fig. S5 and Movie S5), in agreement with experiments in *Anabaena variabilis* (48, 49).

As in experiments (46), overexpression of HetN in our simulations prevents heterocyst differentiation.

We have also simulated the double *patS*:*hetN* knockdown condition. Because in our model only fixed-nitrogen products are working as a weak inhibitor, most of the cells in the filament quickly differentiate into heterocysts, as experimentally observed (47), although as late as after 100 h there is still a small fraction of vegetative cells. Under PatS or HetN overexpression on a *hetN* or *patS* mutant background, respectively, no heterocysts form, as observed (47).

Variance and skewness from our simulations also quantitatively compare well with experimental data (Fig. 4 *B* and *C*). In contrast to the *hetN* mutant, for the wild type and the *patS* mutant skewness diminishes with time, as interval distributions become more symmetric.

Sequestration by PatS and HetN Forms Spatial Gradients of HetR. We have simulated the dynamics of gene expression in the model (Movies S1–S5). Because PatS and HetN (or more accurately, the pentapeptide RGSGR represented by them in our theory) can diffuse along the filament, not surprisingly their profiles can form gradients (64, 65). At early times after nitrogen deprivation, PatS levels increase in the whole filament (8, 23, 39). These levels remain high for some hours, but as some of these cells differentiate into heterocysts, system levels of PatS drop, and eventually high concentrations are observed only at new proto-heterocysts that appear between formed heterocysts when filament growth moves them apart (39). The dynamics of HetN are somewhat reversed. At early times, HetN is not observed (66) because there are no heterocysts that produce it in the filament. At late times, HetN cell concentrations form quasiregular gradients with peaks at heterocysts (46, 67).

HetR concentration levels have been found to form interesting spatial profiles. For instance, expression of *hetR* has been shown to be correlated between neighbor cells before nitrogen deprivation (68). Because HetR does not diffuse, any gradient of its concentration would be produced by its interactions with the gradients of PatS and HetN. In addition, this is precisely what occurs in our model: the expression of HetR shows higher values in cells far apart from heterocysts. The resulting HetR profile shows variability from cell to cell, just as observed experimentally (43). Another prediction of this model is that the dynamics of the border cell is different from those in the middle, due to the accumulation of diffusing peptides at the end of the filament (see Fig. S4*B* for more details).

Quasisynchronous Cell Division Induces Oscillatory Variation of Pattern Properties. The moments of the vegetative interval length distribution show an oscillatory behavior over time, especially the mean and the variance (Fig. 4). The interpeak time in these oscillations is related to the average time for cell division. When vegetative cells divide synchronously, the average distance (and variance) between heterocysts increases. When a new heterocyst appears in the middle of an interval, it divides in two intervals roughly one-half in length. If the cell cycle is roughly synchronous in the whole filament, this mechanism will produce a lengthening of the mean interval with each round of cell division, and a shortening with each round of differentiation. To test this idea, we have made simulations with different levels of noise in cell growth dynamics (Fig. 7*A*). Decreasing the noise, that is, synchronizing cell division, makes the oscillations of the mean interval distance more pronounced. Conversely, increasing the noise makes the oscillations disappear. The effects of the variation of the level of noise for other parameters are shown in *Supporting Information* (Fig. S6).

Quasisynchronous Cell Division Favors Intervals of Even Length. A characteristic property of the heterocyst pattern is the larger frequency of even-numbered vegetative cell intervals with respect to odd ones (58). This is apparent from experimental histograms of interval length in the literature (23, 39, 43, 56–58). Our theory reproduces this observation for wild type and mutants (Fig. 7*B*). The fraction of even intervals also shows an oscillatory behavior over time, a sign that it is also caused by the synchronous character of cell division along the filament. To test this, we plot (Fig. 7*C*) the percentage of even intervals for different levels of noise in cell growth. For weak noise levels in cell growth, synchronous cell division induces a large fraction of even intervals. This fraction drops when interval lengths are large and several differentiation events happen almost simultaneously, randomizing interval parity until a new round of cell division occurs. In contrast, for high noise, rounds of cell division are not even well defined, and the percentage of even intervals remains always close to 50%.

Our result supports previous suggestions (56) that the synchronous division of vegetative cells during the time that new heterocysts are formed is responsible for the higher fraction of even intervals, with no need of extra mechanisms.

Discussion

In this work, we have shown that a model based on a positive-feedback loop that promotes heterocyst differentiation, plus three diffusible inhibitors, an early one with source at protoheterocysts and two late ones with source at heterocysts, is enough to explain the formation and maintenance of heterocyst patterns up to quantitative detail. As suggested by the biochemistry of the system (41), inhibition works through a "multimer cloud" mechanism (69), in which the formation of complexes between activators and

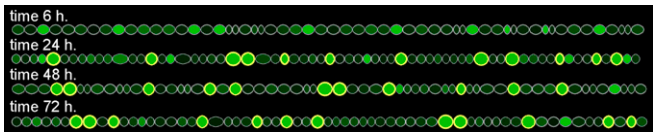

Fig. 6. Temporal evolution of a filament for the *hetN* mutant. Details as in Fig. 2. See also Fig. S3 and Movie S3.

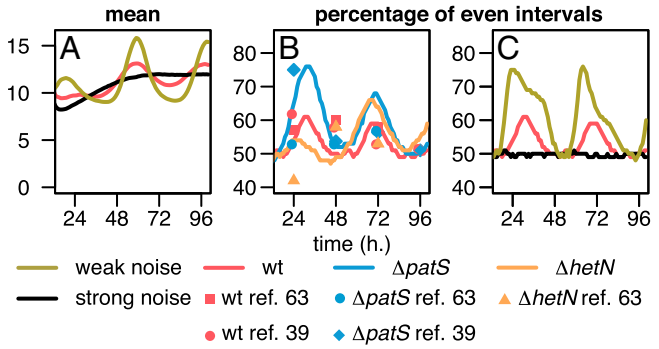

Fig. 7. (*A*) Effect of the noise in cell growth on the mean of the vegetative cells interval distribution. (*B*) Percentage of even intervals for the wild type and *patS* and *hetN* mutants in our model (lines) compared with experiments (symbols) as indicated. (*C*) Effect of the noise in cell growth on the percentage of even intervals. For noise strength parameters, see Tables S1 and S2.

inhibitors sequesters activator complexes and precludes them of realizing their activity. For clarity and concreteness, we have only considered the main genetic regulators of the system, *hetR*, *patS*, and *hetN*, as effective players for local activation, early long-range inhibition, and late long-range inhibition, respectively. A single late inhibitor would produce an overproduction of heterocysts in the *hetN* loss-of-function condition. This suggests the existence of, at least, a second late inhibitor, weaker and diffusing faster than HetN. A plausible candidate is the fixed nitrogen produced by heterocysts.

From a theoretical, more generic perspective, an interesting property of the model is that the main activator for heterocyst differentiation, HetR, is not diffusing. The main mechanisms for the pattern formation and maintenance are the positive-feedback loop for HetR production and diffusion of the inhibitor molecules between cells. The pattern shows a well-defined intrinsic wavelength, robust in time, that does not significantly change due to small variations in model parameter values (see *Supporting Information* for a sensitivity analysis, Fig. S7). This contrasts with the classical Turing continuum model for pattern formation in reactive-diffusive systems (70), where the linear wavelength is proportional to the square root of the product of the activator and inhibitor diffusivities (71). Another main difference with most Turing systems is that the conditions for pattern formation in Turing models need to be finely tuned, and patterns are generally nonrobust in the sense that small variations in parameters may alter the observed wavelength, and even move the system out of the Turing regime. Actually, frequently in the Turing regime different patterns arise at the same point in parameter space, simply owing to slight variations in initial conditions. Obviously, this is not the case in heterocyst pattern formation, where a similar pattern is found independently of environmental and initial conditions.

A key aspect of our work is bringing together regulatory aspects and filament growth through cell division. Without this last aspect, it is possible to create pattern-forming models, but something as important as the maintenance of the pattern cannot be reproduced. Moreover, we show that it is not necessary to consider any cross talk between the cell cycle and the regulation of heterocyst differentiation to reproduce experimental patterns. This cross talk, or some other mechanism, has been postulated as a part of a two-stage model (58), where this mechanism would form a coarse prepattern, from which in a second stage protoheterocysts are refined (22). Our model reproduces quantitatively experimental patterns with a purely stochastic pattern initiation. Both small irregularities in the initial condition or the dynamic noise in the simulations are enough by themselves to trigger the emergence of the pattern. Although a first stage is not needed to form a prepattern, we cannot exclude its existence. Evidence for it has been found in a different strain of cyanobacteria, *Nostoc punctiforme* strain ATCC 29133 (60).

The mechanisms contemplated in our model are only the backbone of this patterning process. The phenotypes of other genes such as *patA* and *hetF* (33, 35–37) show that there is more to the system than local activation and long-range inhibition. Future work should include modeling these finer mechanisms to be able to refine our understanding of how they work and discard hypothesis that do not pass the test of a theory–experiment comparison. Also, extension to different strains of cyanobacteria, and, importantly, use of live gene expression data as in ref. 68 are other main avenues for future work. A better understanding of biochemical kinetics and spatiotemporal aspects of gene expression and metabolite distribution would motivate the construction of models more experimentally constrained. This would allow to use these descriptions to obtain observable predictions and as guides to conduct novel experiments.

ACKNOWLEDGMENTS. We thank Joel Stavans, Fernando Falo, and Jesús Gómez-Gardeñes for enlightening discussions, and Carlos Rascón for critical reading of the manuscript. We acknowledge funding from the Spanish Ministry of Economy and Competitiveness through Grant PHYSDEV (FIS2012-32349) and the Ramón y Cajal Program (to S.A.).

1. Mariscal V, Herrero A, Flores E (2007) Continuous periplasm in a filamentous, heterocyst-forming cyanobacterium. *Mol Microbiol* 65(4):1139–1145.
2. Mullineaux CW, et al. (2008) Mechanism of intercellular molecular exchange in heterocyst-forming cyanobacteria. *EMBO J* 27(9):1299–1308.
3. Zhang LC, Chen YF, Chen WL, Zhang CC (2008) Existence of periplasmic barriers preventing green fluorescent protein diffusion from cell to cell in the cyanobacterium *Anabaena* sp. strain PCC 7120. *Mol Microbiol* 70(4):814–823.
4. Flores E, Herrero A (2010) Compartmentalized function through cell differentiation in filamentous cyanobacteria. *Nat Rev Microbiol* 8(1):39–50.
5. Zhang LC, Risoul V, Latifi A, Christie JM, Zhang CC (2013) Exploring the size limit of protein diffusion through the periplasm in cyanobacterium *Anabaena* sp. PCC 7120 using the 13 kDa iLOV fluorescent protein. *Res Microbiol* 164(7):710–717.
6. Omairi-Nasser A, Haselkorn R, Austin J, 2nd (2014) Visualization of channels connecting cells in filamentous nitrogen-fixing cyanobacteria. *FASEB J* 28(7):3016–3022.
7. Muro-Pastor AM, Hess WR (2012) Heterocyst differentiation: From single mutants to global approaches. *Trends Microbiol* 20(11):548–557.
8. Kumar K, Mella-Herrera RA, Golden JW (2010) Cyanobacterial heterocysts. *Cold Spring Harb Perspect Biol* 2(4):a000315.
9. Wilcox M, Mitchison GJ, Smith RJ (1973) Pattern formation in the blue-green alga, *Anabaena*. I. Basic mechanisms. *J Cell Sci* 12(3):707–723.
10. Wolk CP, Quine MP (1975) Formation of one-dimensional patterns by stochastic processes and by filamentous blue-green algae. *Dev Biol* 46(2):370–382.
11. Meinhardt H (2008) Models of biological pattern formation: From elementary steps to the organization of embryonic axes. *Curr Top Dev Biol* 81:1–63.
12. Pinzon NM, Ju LK (2006) Modeling culture profiles of the heterocystous N_2-fixing cyanobacterium *Anabaena flos-aquae*. *Biotechnol Prog* 22(6):1532–1540.
13. Allard JF, Hill AL, Rutenberg AD (2007) Heterocyst patterns without patterning proteins in cyanobacterial filaments. *Dev Biol* 312(1):427–434.
14. Gerdtzen ZP, et al. (2009) Modeling heterocyst pattern formation in cyanobacteria. *BMC Bioinformatics* 10(Suppl 6):S16.
15. Zhu M, Callahan SM, Allen JS (2010) Maintenance of heterocyst patterning in a filamentous cyanobacterium. *J Biol Dyn* 4(6):621–633.
16. Brown AI, Rutenberg AD (2012) Reconciling cyanobacterial fixed-nitrogen distributions and transport experiments with quantitative modelling. *Phys Biol* 9(1):016007.
17. Brown AI, Rutenberg AD (2012) Heterocyst placement strategies to maximize the growth of cyanobacterial filaments. *Phys Biol* 9(4):046002.
18. Brown AI, Rutenberg AD (2014) A storage-based model of heterocyst commitment and patterning in cyanobacteria. *Phys Biol* 11(1):016001.
19. Torres-Sánchez A, Gómez-Gardeñes J, Falo F (2015) An integrative approach for modeling and simulation of heterocyst pattern formation in cyanobacteria filaments. *PLoS Comput Biol* 11(3):e1004129.
20. Ishihara J, Tachikawa M, Iwasaki H, Mochizuki A (2015) Mathematical study of pattern formation accompanied by heterocyst differentiation in multicellular cyanobacterium. *J Theor Biol* 371:9–23.
21. Asai H, et al. (2009) Cyanobacterial cell lineage analysis of the spatiotemporal *hetR* expression profile during heterocyst pattern formation in *Anabaena* sp. PCC 7120. *PLoS One* 4(10):e7371.
22. Toyoshima M, et al. (2010) Early candidacy for differentiation into heterocysts in the filamentous cyanobacterium *Anabaena* sp. PCC 7120. *Arch Microbiol* 192(1):23–31.

23. Yoon HS, Golden JW (1998) Heterocyst pattern formation controlled by a diffusible peptide. *Science* 282(5390):935–938.
24. Ehira S (2013) Transcriptional regulation of heterocyst differentiation in *Anabaena* sp. strain PCC 7120. *Russ J Plant Physiol* 60(4):443–452.
25. Herrero A, Muro-Pastor AM, Valladares A, Flores E (2004) Cellular differentiation and the NtcA transcription factor in filamentous cyanobacteria. *FEMS Microbiol Rev* 28(4):469–487.
26. Zhang CC, Laurent S, Sakr S, Peng L, Bédu S (2006) Heterocyst differentiation and pattern formation in cyanobacteria: A chorus of signals. *Mol Microbiol* 59(2):367–375.
27. Valladares A, Flores E, Herrero A (2008) Transcription activation by NtcA and 2-oxoglutarate of three genes involved in heterocyst differentiation in the cyanobacterium *Anabaena* sp. strain PCC 7120. *J Bacteriol* 190(18):6126–6133.
28. González A, Valladares A, Peleato ML, Fillat MF (2013) FurA influences heterocyst differentiation in *Anabaena* sp. PCC 7120. *FEBS Lett* 587(16):2682–2690.
29. Buikema WJ, Haselkorn R (1991) Characterization of a gene controlling heterocyst differentiation in the cyanobacterium *Anabaena* 7120. *Genes Dev* 5(2):321–330.
30. Black TA, Cai Y, Wolk CP (1993) Spatial expression and autoregulation of *hetR*, a gene involved in the control of heterocyst development in *Anabaena*. *Mol Microbiol* 9(1):77–84.
31. Haselkorn R (1998) How cyanobacteria count to 10. *Science* 282(5390):891–892.
32. Risser DD, Callahan SM (2007) Mutagenesis of *hetR* reveals amino acids necessary for HetR function in the heterocystous cyanobacterium *Anabaena* sp. strain PCC 7120. *J Bacteriol* 189(6):2460–2467.
33. Buikema WJ, Haselkorn R (2001) Expression of the *Anabaena hetR* gene from a copper-regulated promoter leads to heterocyst differentiation under repressing conditions. *Proc Natl Acad Sci USA* 98(5):2729–2734.
34. Rajagopalan R, Callahan SM (2010) Temporal and spatial regulation of the four transcription start sites of *hetR* from *Anabaena* sp. strain PCC 7120. *J Bacteriol* 192(4): 1088–1096.
35. Liang J, Scappino L, Haselkorn R (1992) The *patA* gene product, which contains a region similar to CheY of *Escherichia coli*, controls heterocyst pattern formation in the cyanobacterium *Anabaena* 7120. *Proc Natl Acad Sci USA* 89(12):5655–5659.
36. Wong FCY, Meeks JC (2001) The *hetF* gene product is essential to heterocyst differentiation and affects HetR function in the cyanobacterium *Nostoc punctiforme*. *J Bacteriol* 183(8):2654–2661.
37. Risser DD, Callahan SM (2008) HetF and PatA control levels of HetR in *Anabaena* sp. strain PCC 7120. *J Bacteriol* 190(23):7645–7654.
38. Higa KC, Callahan SM (2010) Ectopic expression of *hetP* can partially bypass the need for *hetR* in heterocyst differentiation by *Anabaena* sp. strain PCC 7120. *Mol Microbiol* 77(3):562–574.
39. Yoon HS, Golden JW (2001) PatS and products of nitrogen fixation control heterocyst pattern. *J Bacteriol* 183(8):2605–2613.
40. Golden JW, Yoon HS (2003) Heterocyst development in *Anabaena*. *Curr Opin Microbiol* 6(6):557–563.
41. Feldmann EA, et al. (2011) Evidence for direct binding between HetR from *Anabaena* sp. PCC 7120 and PatS-5. *Biochemistry* 50(43):9212–9224.
42. Huang X, Dong Y, Zhao J (2004) HetR homodimer is a DNA-binding protein required for heterocyst differentiation, and the DNA-binding activity is inhibited by PatS. *Proc Natl Acad Sci USA* 101(14):4848–4853.
43. Risser DD, Callahan SM (2009) Genetic and cytological evidence that heterocyst patterning is regulated by inhibitor gradients that promote activator decay. *Proc Natl Acad Sci USA* 106(47):19884–19888.
44. Corrales-Guerrero L, Mariscal V, Flores E, Herrero A (2013) Functional dissection and evidence for intercellular transfer of the heterocyst-differentiation PatS morphogen. *Mol Microbiol* 88(6):1093–1105.
45. Higa KC, et al. (2012) The RGSGR amino acid motif of the intercellular signalling protein, HetN, is required for patterning of heterocysts in *Anabaena* sp. strain PCC 7120. *Mol Microbiol* 83(4):682–693.
46. Callahan SM, Buikema WJ (2001) The role of HetN in maintenance of the heterocyst pattern in *Anabaena* sp. PCC 7120. *Mol Microbiol* 40(4):941–950.
47. Borthakur PB, Orozco CC, Young-Robbins SS, Haselkorn R, Callahan SM (2005) Inactivation of *patS* and *hetN* causes lethal levels of heterocyst differentiation in the filamentous cyanobacterium *Anabaena* sp. PCC 7120. *Mol Microbiol* 57(1):111–123.
48. Thiel T, Pratte B (2001) Effect on heterocyst differentiation of nitrogen fixation in vegetative cells of the cyanobacterium *Anabaena variabilis* ATCC 29413. *J Bacteriol* 183(1):280–286.
49. Thiel T (2004) *Genetics and Regulation of Nitrogen Fixing Bacteria*, eds Klipp W, Masepohl B, Gallon J, Newton W (Kluwer Academic Publishers, Dordrecht, The Netherlands), pp 73–110.
50. Kim Y, et al. (2011) Structure of transcription factor HetR required for heterocyst differentiation in cyanobacteria. *Proc Natl Acad Sci USA* 108(25):10109–10114.
51. Kim Y, et al. (2013) Structures of complexes comprised of *Fischerella* transcription factor HetR with *Anabaena* DNA targets. *Proc Natl Acad Sci USA* 110(19):E1716–E1723.
52. Valladares A, Flores E, Herrero A (2016) The heterocyst differentiation transcriptional regulator HetR of the filamentous cyanobacterium *Anabaena* forms tetramers and can be regulated by phosphorylation. *Mol Microbiol* 99(4):808–819.
53. Hu HX, et al. (2015) Structural insights into HetR-PatS interaction involved in cyanobacterial pattern formation. *Sci Rep* 5:16470.
54. Zhou R, Cao Z, Zhao J (1998) Characterization of HetR protein turnover in *Anabaena* sp. PCC 7120. *Arch Microbiol* 169(5):417–423.
55. Jang J, Shi L, Tan H, Janicki A, Zhang CC (2009) Mutual regulation of *ntcA* and *hetR* during heterocyst differentiation requires two similar PP2C-type protein phosphatases, PrpJ1 and PrpJ2, in *Anabaena* sp. strain PCC 7120. *J Bacteriol* 191(19):6059–6066.
56. Khudyakov IY, Golden JW (2004) Different functions of HetR, a master regulator of heterocyst differentiation in *Anabaena* sp. PCC 7120, can be separated by mutation. *Proc Natl Acad Sci USA* 101(45):16040–16045.
57. Wu X, Liu D, Lee MH, Golden JW (2004) *patS* minigenes inhibit heterocyst development of *Anabaena* sp. strain PCC 7120. *J Bacteriol* 186(19):6422–6429.
58. Meeks JC, Elhai J (2002) Regulation of cellular differentiation in filamentous cyanobacteria in free-living and plant-associated symbiotic growth states. *Microbiol Mol Biol Rev* 66(1):94–121.
59. Young-Robbins SS, Risser DD, Moran JR, Haselkorn R, Callahan SM (2010) Transcriptional regulation of the heterocyst patterning gene *patA* from *Anabaena* sp. strain PCC 7120. *J Bacteriol* 192(18):4732–4740.
60. Risser DD, Wong FCY, Meeks JC (2012) Biased inheritance of the protein PatN frees vegetative cells to initiate patterned heterocyst differentiation. *Proc Natl Acad Sci USA* 109(38):15342–15347.
61. Orozco CC, Risser DD, Callahan SM (2006) Epistasis analysis of four genes from *Anabaena* sp. strain PCC 7120 suggests a connection between PatA and PatS in heterocyst pattern formation. *J Bacteriol* 188(5):1808–1816.
62. Corrales-Guerrero L, et al. (2014) Subcellular localization and clues for the function of the HetN factor influencing heterocyst distribution in *Anabaena* sp. strain PCC 7120. *J Bacteriol* 196(19):3452–3460.
63. Corrales-Guerrero L, Flores E, Herrero A (2014) Relationships between the ABC-exporter HetC and peptides that regulate the spatiotemporal pattern of heterocyst distribution in *Anabaena*. *PLoS One* 9(8):e104571.
64. Kholodenko BN (2006) Cell-signalling dynamics in time and space. *Nat Rev Mol Cell Biol* 7(3):165–176.
65. Muñoz-García J, Kholodenko BN (2010) Signalling over a distance: Gradient patterns and phosphorylation waves within single cells. *Biochem Soc Trans* 38(5):1235–1241.
66. Bauer CC, et al. (1997) Suppression of heterocyst differentiation in *Anabaena* PCC 7120 by a cosmid carrying wild-type genes encoding enzymes for fatty acid synthesis. *FEMS Microbiol Lett* 151(1):23–30.
67. Li B, Huang X, Zhao J (2002) Expression of *hetN* during heterocyst differentiation and its inhibition of *hetR* up-regulation in the cyanobacterium *Anabaena* sp. PCC 7120. *FEBS Lett* 517(1-3):87–91.
68. Corrales-Guerrero L, et al. (2015) Spatial fluctuations in expression of the heterocyst differentiation regulatory gene *hetR* in *Anabaena* filaments. *PLoS Genet* 11(4):e1005031.
69. Schröter C, et al. (2012) Topology and dynamics of the zebrafish segmentation clock core circuit. *PLoS Biol* 10(7):e1001364.
70. Turing AM (1952) The chemical basis of morphogenesis. *Philos Trans R Soc B* 237(641): 37–72.
71. Murray JD (2001) *Mathematical Biology. II Spatial Models and Biomedical Applications* (Springer, New York).
72. Spinner DS, Liu S, Wang SW, Schmidt J (2002) Interaction of the myogenic determination factor myogenin with E12 and a DNA target: Mechanism and kinetics. *J Mol Biol* 317(3):431–445.
73. Frigola D, Casanellas L, Sancho JM, Ibañes M (2012) Asymmetric stochastic switching driven by intrinsic molecular noise. *PLoS One* 7(2):e31407.
74. Kloeden PE, Platen E (1992) *Numerical Solution of Stochastic Differential Equations* (Springer, Berlin).
75. Savageau MA (1971) Parameter sensitivity as a criterion for evaluating and comparing the performance of biochemical systems. *Nature* 229(5286):542–544.

Supporting Information

Muñoz-García and Ares 10.1073/pnas.1524383113

Model Construction

We have constructed a model consisting of four variables per cell representing the concentration in the cell of molecular species responsible for the mechanisms of local autoactivation, early long-range inhibition and two types, strong and weak, of late long-range inhibition. We identify the molecules responsible for these mechanisms with HetR, PatS, HetN, and fixed-nitrogen products, and base the reaction scheme between the genes (Fig. 1 of the main text) on the biochemistry discussed in ref. 41. The identification of the weak late inhibitor with fixed-nitrogen products is speculative. However, they are a strong candidate to play this role, and in the following we will refer to them when discussing this mechanism. For simplicity, we do not describe mRNA concentrations and, for each cell i, have four variables: h_i for the concentration of HetR monomers, p_i for the concentration of PatS monomers, n_i for the concentration of HetN monomers, and f_i for the concentration of fixed-nitrogen products.

In our model, we distinguish between vegetative cells and heterocysts. In vegetative cells, HetN is not produced. HetR is produced with a small constitutive rate (34). Its monomers can bind into dimers (42, 50, 51). These HetR dimers can bind the *hetR* and *patS* promoter regions and activate production of HetR and PatS. If the concentration of HetR builds up above a threshold value without ever falling below a certain minimum value, the vegetative cell differentiates and turns into a heterocyst. Because heterocysts have already differentiated and HetR cannot diffuse between cells in our model, modeling HetR concentration in them is superfluous. However, because experimentally HetR concentration in heterocysts is high, we model it with a constitutive term. Heterocysts do not produce PatS, but HetN and fixed-nitrogen products are produced with a constitutive rate.

The RGSGR pentapeptide, a product of PatS, can bind HetR with a 1:1 stoichiometry, and RGSGR-tagged HetR molecules can no longer bind DNA (41). We assume the concentration of RGSGR derived from PatS is proportional to p_i. HetN also contains a RGSGR motif (45), so as with PatS, we assume the concentration of RGSGR derived from HetN is proportional to n_i. We allow the RGSGR pentapeptide to diffuse between neighbor cells, irrespectively of their vegetative or heterocyst identity. Because of this, we can find nonzero levels of p_i in heterocysts or nonzero levels of n_i in vegetative cells. Finally, we assume that HetR dimers tagged with one or two RGSGR molecules can no longer bind DNA (41). Hence, inhibition of HetR activity by PatS or HetN would be due to sequestration or titration of HetR dimers. This is similar to the "cloud of dimers" mechanism that appears in other biological processes (69).

Fixed-nitrogen products are assumed to diffuse between cells much faster than the RGSGR pentapeptide and be weaker inhibitors than HetN and PatS.

Mathematical Formalism

The model description above can be used to write a set of chemical reactions for the following species: HetR monomers, HetR dimers (HetR:HetR), PatS monomers, HetN monomers, fixed-nitrogen products, and the complexes HetR:HetR:PatS, HetR:HetR:HetN, HetR:HetR:Pats:PatS, HetR:HetR:HetN:HetN, and HetR:HetR:PatS:HetN. PatS and HetN in the complexes actually represent RGSGR molecules. Only monomers can be produced by transcription and translation (bundled into a single process). We consider linear degradation kinetics for both monomers and multimers. Formation of a complex between HetR:HetR and the promoter regions of *hetR* and *patS* in vegetative cells is also considered. The formation of these complexes increases the rate of HetR and PatS production, respectively. The effect of fixed-nitrogen products is included in a phenomenological way as an inhibition in the regulatory function controlling the production rate of HetR and PatS. Assuming mass-action kinetics, we can write differential equations for the time evolution of each species. Making the usual assumption that all of the multimer reactions (binding and unbinding of monomers) are much faster than degradation reactions (72), we can make an adiabatic approximation and eliminate all multimer concentrations from the description. The resulting kinetics for monomer concentrations are as follows:

$$\frac{dh_i(t)}{dt} = b_h + a_h g(h_i,p_i,n_i,f_i) - \alpha_h h_i(t)[1+2\mu h_i(t)], \quad \text{[S1]}$$

$$\frac{dp_i(t)}{dt} = b_p + [1-\delta_{\mathrm{hc},i}]a_p g(h_i,p_i,n_i,f_i) - \alpha_p p_i(t) + d_p[p_{i+1}(t) - 2p_i(t) + p_{i-1}(t)], \quad \text{[S2]}$$

$$\frac{dn_i(t)}{dt} = b_n + \delta_{\mathrm{hc},i}a_n - \alpha_n n_i(t) + d_n[n_{i+1}(t) - 2n_i(t) + n_{i-1}(t)], \quad \text{[S3]}$$

$$\frac{df_i(t)}{dt} = b_f + \delta_{\mathrm{hc},i}a_f - \alpha_f f_i(t) + d_f[f_{i+1}(t) - 2f_i(t) + f_{i-1}(t)], \quad \text{[S4]}$$

with

$$g(h_i,p_i,n_i,f_i) = \frac{\left[\frac{h_i(t)}{k}\right]^2}{1+\left[\frac{h_i(t)}{k}\right]^2 + \frac{p_i(t)}{K_d} + \frac{n_i(t)}{K_d} + \left[\frac{p_i(t)}{K_d}\right]^2 + \left[\frac{n_i(t)}{K_d}\right]^2 + \frac{p_i(t)n_i(t)}{K_d^2} + \frac{f_i(t)}{K_f}}. \quad \text{[S5]}$$

The subindex i means that the variable is referred to cell i in the filament, its neighbor cells are $i-1$ and $i+1$ (cells at the extremes of the filament only have one neighbor), t denotes time, h_i is the HetR concentration in cell i, p_i is the PatS concentration, n_i is the *HetN* concentration, and f_i is the fixed-nitrogen products concentration. In a parameter, the subindex h means that it is related to variable h_i, p to p_i, n to n_i, and f to f_i. b_h, b_p, b_n, and b_f are basal or constitutive production rates; we have used $b_p = b_n = b_f = 0$, but checked that the model is robust to finite values of these parameters. a_h, a_p, a_n, and a_f are the maximum regulated production rates. α_h, α_p, α_n, and α_f are linear degradation rates. d_p, d_n, and d_f are intercellular diffusion rates. We take the concentration of each species to be homogeneous inside a cell. The nonlinear degradation term in the equation for h_i appears as the effect of dimer-mediated degradation of monomers (69). The parameter μ is related to the rates k_b of HetR monomers binding to form HetR dimers, k_u of HetR dimers unbinding into HetR monomers, α_d of dimer degradation, and α_h of monomer degradation as follows:

$$\mu = \frac{k_b}{\alpha_h}\left(1 - \frac{k_u}{k_u + \alpha_d}\right). \quad \text{[S6]}$$

The factor $\delta_{\mathrm{hc},i}$ specifies whether the cell is vegetative or a heterocyst: its value is 1 if cell i is a heterocyst, and 0 if it is vegetative. Because heterocysts cannot divide, initially all cells are

vegetative and have $\delta_{\mathrm{hc},i}=0$; it changes to $\delta_{\mathrm{hc},i}=1$ if at any point the cell differentiates into a heterocyst. Regulation of the production of h_i and p_i is done through the function $g(h_i,p_i,n_i,f_i)$ specified in Eq. **S5**. k is the equilibrium constant (or dissociation constant) of the binding–unbinding reaction between the HetR dimer and the *hetR* and *patS* promoters; for simplicity, we take both these constants to have the same value. K_d is the equilibrium constant for the binding–unbinding reaction between HetR and the RGSGR pentapeptide. Its value has been measured experimentally for PatS-derived RGSGR: $K_d=227\pm23$ nM (41). We assume the same value for HetN-derived RGSGR. The different terms with K_d in the denominator of Eq. **S5** come from the titration of HetR dimers by a single PatS-derived RGSGR molecule, a single HetN-derived RGSGR molecule, two PatS-derived RGSGR molecules, two HetN-derived RGSGR molecules, and one PatS-derived plus a HetN-derived RGSGR molecules, respectively. The function could have been approximated by a simpler one where only the p_i^2 and n_i^2 terms related to K_d would be taken into account: this would have not changed the dynamics of the model in any relevant way. For the effective constant K_f controlling the strength of HetR and PatS repression by fixed-nitrogen products, we have chosen to use the same value as for K_d. Taking $K_f=K_d$ may be unrealistic. However, the strength of the effect of the fixed-nitrogen products is given by both K_f and by its production rate a_f. To make this inhibition effect weaker than the effect of HetN, we have set the production rate of the fixed-nitrogen products to be much lower than the production rate of HetN, $a_f \ll a_n$.

Model Implementation

We have implemented a code in an object-oriented platform to model the differentiation and growth of vegetative and heterocyst cells. In this programming environment, each cell is described by an agent that has its own variables representing cell size and the current concentration of the species considered, HetR, PatS, HetN, and fixed-nitrogen products. These agents are ordered in a structure representing the filament. Because there can be a net flux of protein concentration between cells, the evolution equations for each agent are coupled with the equations for its adjacent neighbors. Cells at the extremes of the filament only have one neighbor. The evolution of the protein and fixed-nitrogen products concentrations for each cell is based on the noisy version of Eqs. **S1–S4**. The stochastic nature of gene expression has been considered in our model by extending the equations derived above to the Langevin dynamics in the Itô interpretation (73). Because the evolution for a given concentration at cell i, x_i, consists on a sum of production (synthesis) terms, P_i, minus the sum of degradation terms, D_i, a stochastic term of the form $\eta_{xi}(t)\sqrt{P_{xi}+|D_{xi}|}$ was included in Eqs. **S1–S3**. Here, $\eta_{xi}(t)$ is an uncorrelated Gaussian white noise with zero mean and variance $\langle\eta_{xi}(t)\eta_{xi'}(t')\rangle=\delta_{ii'}\delta(t-t')/V$, where V is an nondimensional effective volume setting noise strength in gene expression (73).

Vegetative cell growth was modeled by a stochastic differential equation for each agent:

$$\frac{ds_i(t)}{dt}=\rho+\eta_{si}(t), \qquad \textbf{[S7]}$$

where s_i is the size of cell i, ρ is a constant growth rate, and $\eta_{si}(t)$ is an uncorrelated Gaussian white noise with zero mean and variance $\langle\eta_{si}(t)\eta_{si'}(t')\rangle=G\delta_{ii'}\delta(t-t')$, which models the intrinsic fluctuations in the growth process. Starting from an initial size, each cell evolves following Eq. **S7** up to a maximum size η_{di}, which is a noisy value drawn from a Gaussian distribution for each cell. When this size is reached, the vegetative cell divides, producing two new vegetative cells with one-half of its current size and identical protein concentrations. Heterocysts grow following the same dynamics, but once reached their maximum size, η_{di}, they do not divide and stop growing.

To differentiate into a heterocyst, a vegetative cell has to build up a certain level of HetR. This has been implemented integrating over time for each vegetative cell the value of HetR concentration, once the value of h_i is above a threshold η_{rs}. This threshold is cell specific, being drawn from a Gaussian distribution. If at any point the value of h_i drops below η_{rs}, the integral is reset to zero. Otherwise, if the integral ever reaches a value η_{ci}, also a cell-specific Gaussian distributed parameter, the vegetative cell differentiates into a heterocyst and $\delta_{\mathrm{hc},i}$ changes from 0 to 1. An alternative way to model the differentiation decision is to consider that, if h_i is above a given threshold for a certain window of continuous time, that particular vegetative cell will transform into a heterocyst. We checked this procedure, using the same threshold η_{rs} listed in Table S2 and a time window of 8 h, which has produced results indistinguishable from the method based on integrating the concentration over time.

Numerical integration of the equations has been made using the Euler–Maruyama approximation for stochastic differential equations (74). Each simulation starts with 150 cells of size 3.3 μm, and initial concentrations at each cell $p_i(0)=n_i(0)=0$ nM and a noisy value drawn from a Gaussian distribution with mean 9.4 and SD 0.2 nM for $h_i(0)$. No-flux boundary conditions were employed. The beginning of the simulation represents the moment of nitrogen deprivation. The statistical results in this work come from an average over 192 different realizations.

To simulate loss-of-function conditions, we have made the relevant parameters equal to zero. For instance, for the *patS* loss-of-function condition, we used $a_p=0$ nM/h, ensuring no PatS production. Overexpression is simulated setting the corresponding basal production rate equal to the maximum regulated production rate.

To calculate the mean, variance, and skewness of vegetative cell intervals (Fig. 4 of the main text), we have not considered intervals of length 0, frequent in a Mch phenotype. The reason to do this is to allow comparison with experimental references that do not report this piece of information.

Parameter Estimation

Some parameters were obtained from literature. The affinity of RGSGR to HetR, K_d, was taken directly from ref. 41. We consider that cells that have just divided are about 2 μm long and roughly double their size before division. With these numbers, we have considered a cellular growth rate of $\rho=0.05$ μm/h, which produces a mean generation time of 40 h, in agreement with the data from ref. 56 analyzed in ref. 13. All of the other parameters were chosen with the aim to quantitatively reproduce the observations of the heterocyst pattern dynamics for the wild-type and mutant phenotypes. A preliminary linear stability analysis of a continuous version of Eqs. **S1–S5** was performed to establish a valid range of parameters in which the homogeneous steady state of the system is unstable and a spatial pattern in the protein concentration levels appears. Parameter values used in the wild-type simulation are given in Table S1.

Together with the dynamic noise in gene expression and cell growth, some parameters have cell-specific values obtained from a Gaussian distribution using the Box–Muller algorithm. The mean and SD of these parameters are given in Table S2.

Temporal Evolution of Gene Expression in the Filaments

Figs. S1–S3 and S5 show the expression of all four species considered in the model for different conditions at 6, 12, 24, 48, and 72 h after nitrogen deprivation. Some of the main features of the temporal evolution of these concentrations for each phenotype have been already discussed in the main text. For instance, as already stressed there, high levels of PatS are found for the wild type at short times (Fig. S1). However, PatS concentrations decrease with time, and, eventually, large gradients of PatS are found only around protoheterocysts at long times. The dynamics

of HetN is different. Gradients of HetN are only observed next to heterocysts at late times. Regarding the differences between wild type and mutants, HetR levels are larger in the *patS* mutant than in the wild type and *hetN* mutant at short times, coming back to low levels after a few hours (Fig. S2). This agrees with experimental observations (23, 39). Another main difference between the wild-type and the mutant phenotypes is that the appearance of contiguous heterocysts is more common in the mutants. However, in contrast to the early contiguous heterocysts in the *patS* mutant, in the *hetN* mutant they form at later times (Fig. S3). Thus, if we inspect a *hetN* mutant a long time after nitrogen deprivation, a large amount of contiguous heterocysts can be found.

Differentiation of Border Cells

The cells at the border of a filament are an interesting study case, because the possible accumulation of diffusing peptides may render their dynamics different from those of the cells in the middle of a filament. An extreme case is the *patA* mutant, in which mainly the border cells of the filament differentiate into heterocysts (33, 35, 37). In Fig. S4*B*, we plot the frequency of heterocyst formation both in the whole filament and considering only the two border cells, for wild type, *patS* loss of function, hetN loss of function, and no late long-range inhibitors. In all cases, the probability of a border cell being a heterocyst grows over time, because once a border cell differentiates it will remain a heterocyst forever.

Regarding the wild type, border cells initially have a lower propensity to differentiate than other cells. This is due to the fact that no-flux boundary conditions were used in our model. Therefore, PatS does not diffuse at the borders and accumulates at them, which has an inhibitory effect on differentiation. However, once the first round of differentiation has occurred, the main role inhibiting differentiation is played by HetN, which is only produced in heterocysts and diffuses to their neighbor cells. Now, a border cell will be the one in its vegetative interval that is further away from the first heterocyst, so as cell division goes on moving that heterocyst further away from it, it will be the cell with higher chances to differentiate. For this reason, the probability of a border cell to become a heterocyst becomes larger than in the interior of the filament.

The initial situation in a *hetN* mutant is very similar to the wild type. However, after the first round of differentiation, the inhibitory effect on heterocyst formation occurs only through PatS and fixed-nitrogen products. The latter diffuses very fast and has an almost homogeneous distribution along the filament, so it does not significantly increase the border cell's advantage to differentiate over the rest of the cells. Thus, the initial situation for the cells at the end of the filaments of having a smaller probability of transforming into a heterocyst is maintained due to PatS accumulation. For this reason, in *hetN* mutants, border heterocysts are less frequent than interior heterocysts.

The situation with no late inhibitors of any kind at early times is again similar to wild type, but as time goes by the probability to differentiate at the borders grows dramatically, just as in cells in the interior of the filament (Fig. S4*A*).

In *patS* mutants, due to the lack of PatS accumulation at the borders, right after nitrogen deprivation there is not any inhibitor that stops a border cell from differentiating. Moreover, after the formation of the first generation of heterocysts, as in the wild type, the effect produced by HetN favors even higher probability of differentiation at the borders. Fig. S4*B* shows that our simulations predict a very high frequency of border heterocysts in *patS* mutants.

In summary, PatS and HetN have opposite effects on the probability of a border cell to become a heterocyst. Due to its accumulation at the borders in this theoretical model, PatS diminishes this probability. For HetN, because cells at the ends of the filament are the ones further away from the first heterocyst producing HetN, their probability to become heterocysts is larger than for the rest of the cells. It would be very interesting to check these predictions with experimental observations.

Noise Effects

In the simulations shown in Fig. 7 *A* and *C* of the main text, three different pairs of values of the intrinsic noise in cell growth G and the SD of the maximum cell size η_{di} were used to reproduce weak, medium, and strong noise conditions in cellular growth. The values of the parameters or their SDs used for the weak and strong conditions in these simulations, and for the conditions discussed throughout this section, are indicated in parentheses in Tables S1 and S2.

We have also studied the effect of variability on G and η_{di} independently. Weak and strong noise in cell growth and maximum cell size have a similar effect as that observed in Fig. 7*A* of the main text. Small values of these noises induce large oscillations in the mean interval distance between heterocysts. Large values decrease these oscillations (see, for example, Fig. S6*A* for small and large deviations for the maximum cell size, η_{di}).

Increasing variation in the threshold, parameters η_{rs} and η_{ci} used to decide when a cell differentiates, produces a small decrease of the interval mean (Fig. S6*B*). With a less homogeneous threshold, it is more probable that protoheterocysts close to mature heterocysts have small values of this threshold and differentiate easily. More regular and longer intervals are found with a weak variation in this parameter.

A similar effect as for the variation in η_{rs} is found for the stochasticity in gene expression. Strong noise (small values of V) produces a decrease in the mean interval length (Fig. S6*C*). That is because large noise in gene expression dynamics makes it easier for protoheterocysts to reach high values of HetR concentration and differentiate, which leads to shorter vegetative intervals. Although there is no experimental data to make comparisons, a more detailed study of noise effects could represent an interesting direction for future work.

Sensitivity Analysis and Robustness

We have performed a sensitivity analysis of the model (75) and find that the mean distance between heterocysts and other pattern features are robust in time and with respect to changes in model parameter values. The model is more sensitive to alterations in those parameters related to *hetR* production and degradation rates, and its affinity to promoters, stressing the importance of the HetR local positive feedback, and confirming that *hetR* acts as the master regulator of the process. In any case, for the parameter ranges considered, the system shows a stable heterocyst pattern with a well-defined wavelength for any initial and boundary conditions.

We define the sensitivity S_{YX} of the observable Y with respect to changes in the parameter X as follows:

$$S_{YX} = \frac{\partial \log Y}{\partial \log X}. \qquad \textbf{[S8]}$$

This quantity is evaluated at some point in the parameter space. The logarithmic derivative defined above can be written as follows:

$$S_{YX} = \frac{dY/Y}{dX/X}. \qquad \textbf{[S9]}$$

To compute the sensitivity for small changes in the parameter X, we approximate Eq. **S9** by the ratio of relative changes as follows:

$$S_{YX} = \frac{\Delta Y/Y}{\Delta X/X}. \qquad \textbf{[S10]}$$

We determine the sensitivity of the model to changes in a given parameter X by evaluating the selected observable Y at two points,

the focal point X_0 and $X = X_0 + \Delta X$. The sensitivity, S_{YX}, thus defined is the ratio between the percentage change in the variable Y and the percentage change in the parameter X.

We have studied the model sensitivity and robustness by performing multiple simulations for all of the parameters in our model and checking how the parameters affect the main pattern characteristics. We show the results regarding the mean distance between heterocysts, as one of the most relevant features of the heterocyst pattern (Fig. S7). We find that the model is most sensitive with respect to *hetR* production and degradation rates, and its affinity to promoters. The model is very robust to small variations of any other parameter. This shows that the local positive feedback is the master regulator of the process, and we have used this fact to fit the model to experimental results using the three key parameters as the main handles to pattern properties.

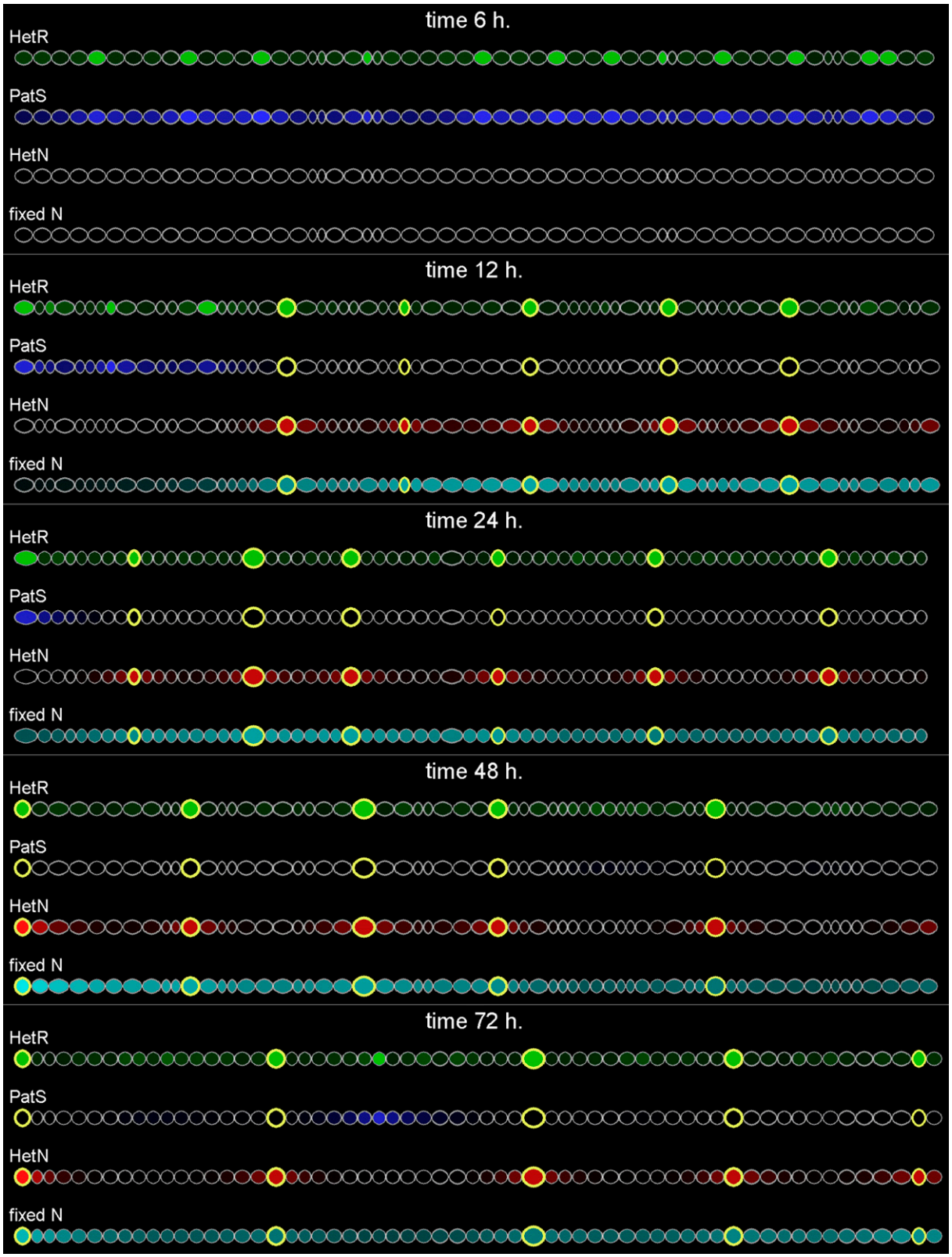

Fig. S1. Temporal evolution of gene expression in a filament for wild type, depicted at 6, 12, 24, 48, and 72 h after nitrogen deprivation. Heterocyst cells have a yellow membrane. The intensity of the green, blue, red, and cyan colors show the level of HetR, PatS, HetN, and fixed-nitrogen products concentrations, respectively. For convenience, to occupy a single line, only the initial part of the filament is shown. See also Movie S1.

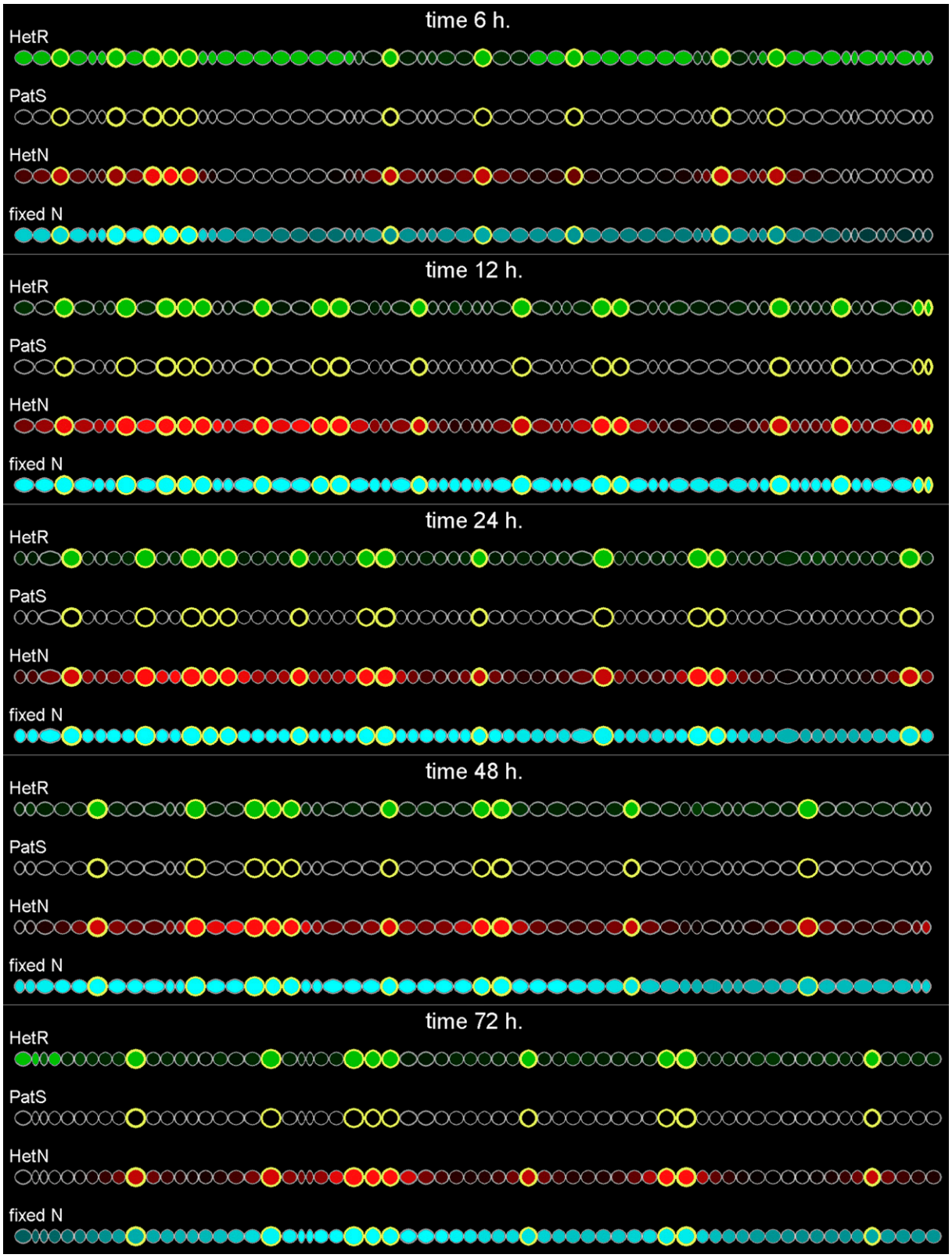

Fig. S2. Temporal evolution of gene expression in a filament for *patS* loss of function. Details as in Fig. S1. See also Movie S2.

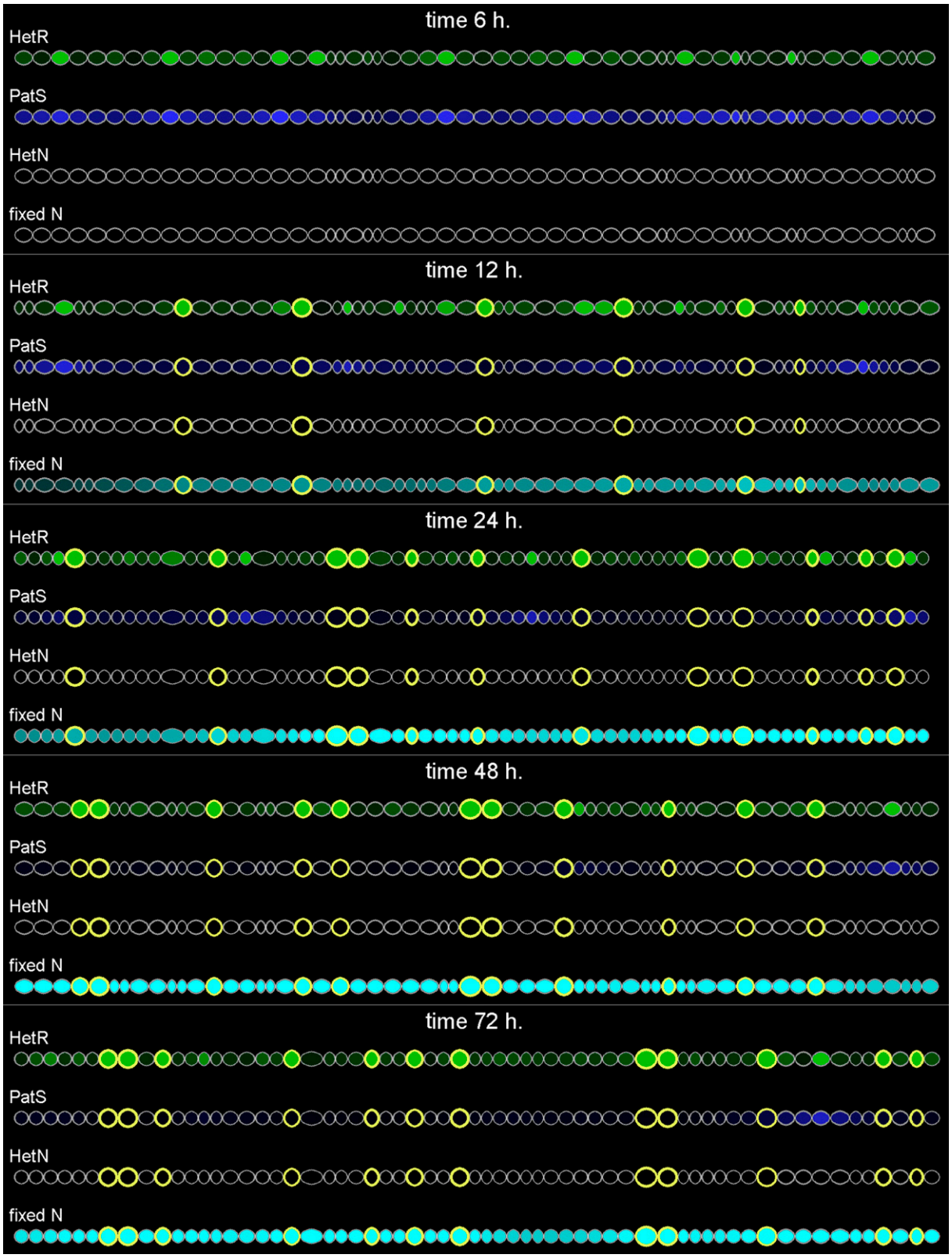

Fig. S3. Temporal evolution of gene expression in a filament for *hetN* loss of function. Details as in Fig. S1. See also Movie S3.

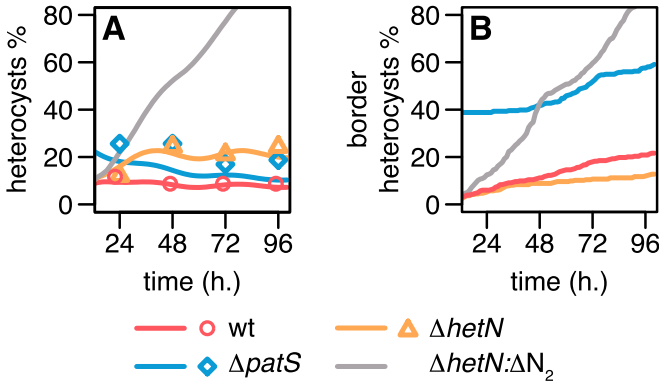

Fig. S4. Dynamics of the percentage of heterocysts. (*A*) Time evolution of the percentage of heterocyst cells in our model (lines) and experimental results in ref. 47 (symbols). Red and circles for wild type, blue and diamonds for *patS* loss of function, orange and triangles for *hetN* loss of function, and gray for no late long-range inhibitors. (*B*) Time evolution of the percentage of heterocysts in border cells in our model.

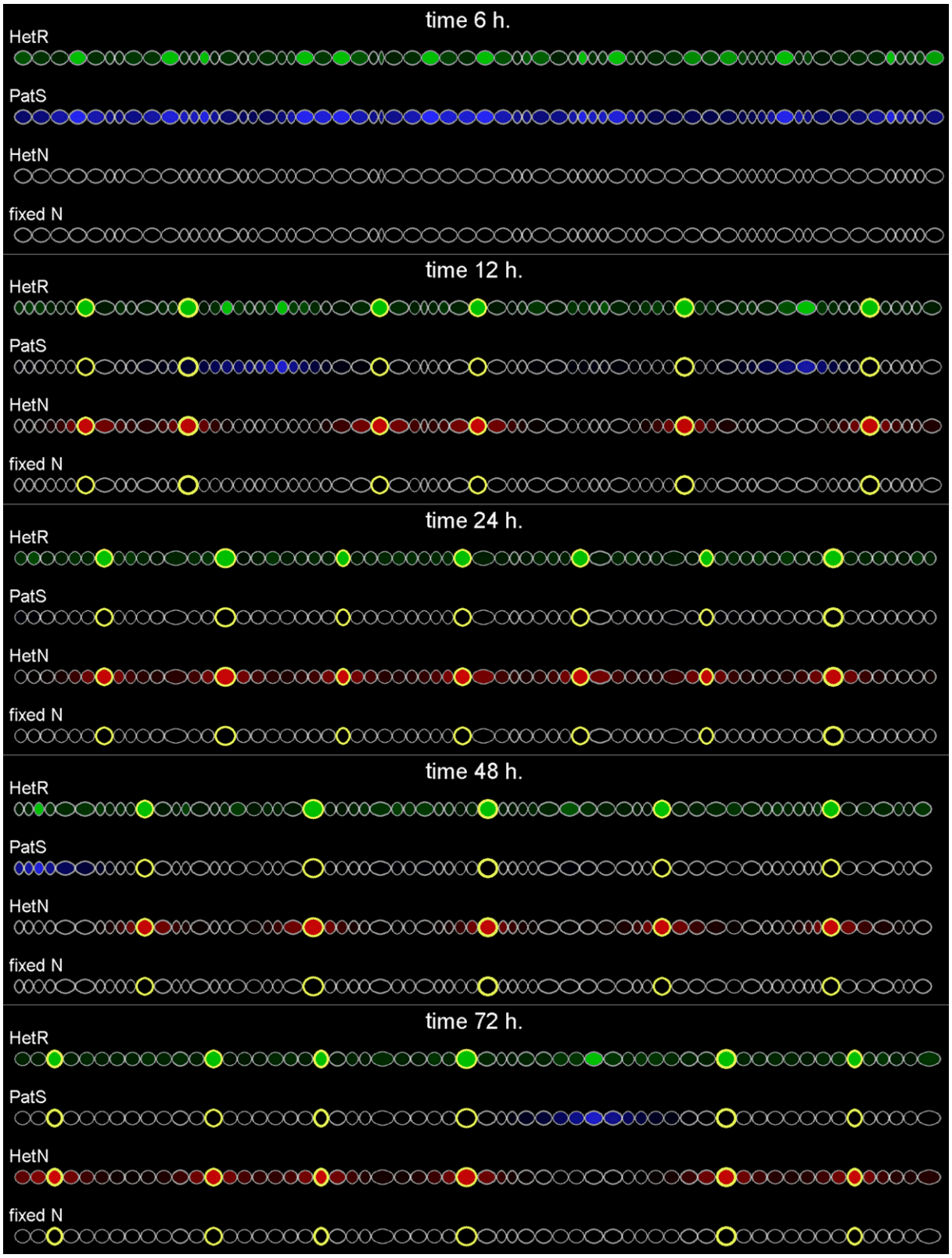

Fig. S5. Temporal evolution of gene expression in a filament for fixed-nitrogen loss of function. Details as in Fig. S1. See also Movie S5.

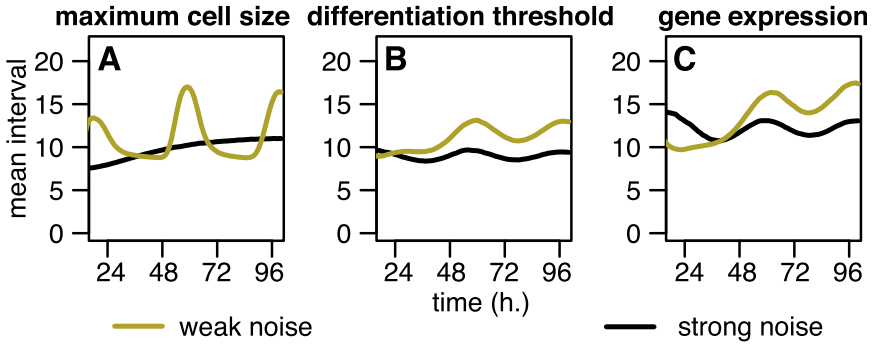

Fig. S6. Effect of noise on the mean of the vegetative cells interval distribution. Noise in (*A*) η_{di}, the maximum cell size for division; (*B*) η_{rs} and η_{ci}, the maximum cumulative level and minimum reset level for differentiation; and (*C*) gene expression, given by the value of V^{-1}. Weak and strong stand for conditions with less and more variability than our wild-type parameters, respectively. Parameter values for these conditions are given in Tables S1 and S2.

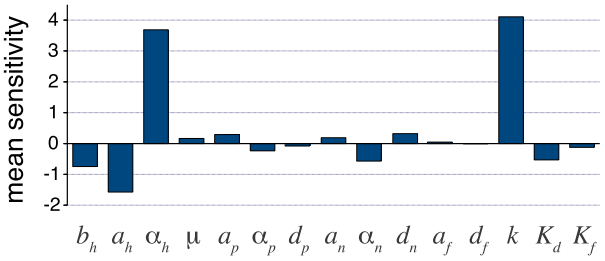

Fig. S7. Sensitivity of the mean distance between heterocysts after 96 h with respect to 10% changes in the indicated parameter values. This analysis is computed at the same point in parameter space used to describe the wild-type phenotype (Table S1).

Table S1. Parameters used in wild-type simulations

Parameter	Description	Value	Units
b_h	HetR basal production rate	37.5	$nM{\cdot}h^{-1}$
a_h	HetR maximum regulated production rate	1,500	$nM{\cdot}h^{-1}$
α_h	HetR degradation rate	4	h^{-1}
μ	HetR dimer-mediated degradation rate	0.001	nM^{-1}
b_p	PatS basal production rate	0	$nM{\cdot}h^{-1}$
a_p	PatS maximum regulated production rate	3,000	$nM{\cdot}h^{-1}$
α_p	PatS degradation rate	2	h^{-1}
d_p	PatS diffusion rate	10	h^{-1}
b_n	HetN basal production rate	0	$nM{\cdot}h^{-1}$
a_n	HetN production rate in heterocysts	12,000	$nM{\cdot}h^{-1}$
α_n	HetN degradation rate	2.5	h^{-1}
d_n	HetN diffusion rate	7.5	h^{-1}
b_f	Fixed-nitrogen basal production rate	0	$nM{\cdot}h^{-1}$
a_f	Fixed-nitrogen production rate in heterocysts	1,000	$nM{\cdot}h^{-1}$
α_f	Fixed-nitrogen degradation rate	2.5	h^{-1}
d_f	Fixed-nitrogen diffusion rate	150	h^{-1}
k	Affinity of HetR dimer to promoter	100	nM
K_d	Affinity of RGSGR to HetR	227 (ref. 41)	nM
K_f	Effective affinity of fixed nitrogen to HetR	227	nM
ρ	Cellular growth rate	0.05	$\mu m{\cdot}h^{-1}$
V^{-1}	Noise strength in gene expression	0.8 (0.05, 5)	Dimensionless
G	Variance of noise in cellular growth	2.5 (0.6, 5.5) $\times 10^{-4}$	$\mu m{\cdot}h^{-1}$

Values in parentheses for V^{-1} and G are those used for the weak and strong noise conditions (Fig. 7 of the main text and Fig. S6).

Table S2. Stochastic terms used in wild-type simulations

Parameter	Noise description	Mean	SD	Units
η_{di}	Maximum size for cell division	4	0.42 (0.21, 0.84)	μm
η_{ci}	Maximum cumulative level for differentiation	960	192 (64, 576)	nM·h
η_{rs}	Minimum threshold level for differentiation reset	60	12 (4, 36)	nM

Values in parentheses are those used for the weak and strong noise conditions (Fig. 7 of the main text and Fig. S6).

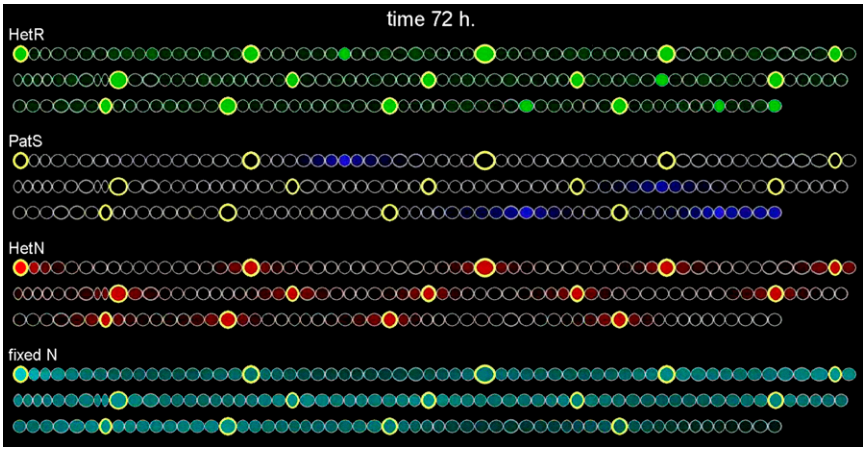

Movie S1. Temporal evolution of gene expression in a filament for wild type. Time counts hours after nitrogen deprivation. Heterocyst cells have a yellow membrane. The intensity of the green, blue, red, and cyan colors show the level of HetR, PatS, HetN, and fixed-nitrogen products concentrations, respectively. When a filament is too long to fit in the width of the movie, it is continued in a row below. The last cell on the right of a row is a neighbor of the first cell on the left of the row immediately below.

Movie S1

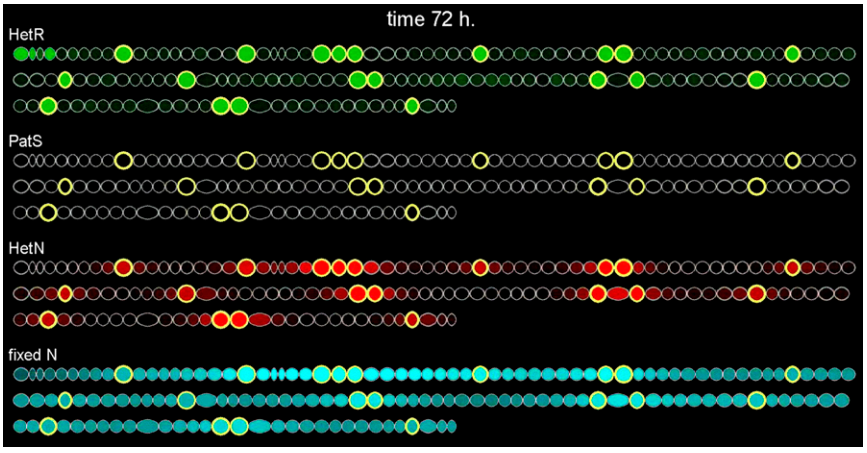

Movie S2. Temporal evolution of gene expression in the filament for *patS* loss of function. Time counts hours after nitrogen deprivation. Heterocyst cells have a yellow membrane. The intensity of the green, red, and cyan colors show the level of HetR, HetN, and fixed-nitrogen products concentrations, respectively. In the second line, cells are black because they do not express PatS. When a filament is too long to fit in the width of the movie, it is continued in a row below. The last cell on the right of a row is a neighbor of the first cell on the left of the row immediately below.

Movie S2

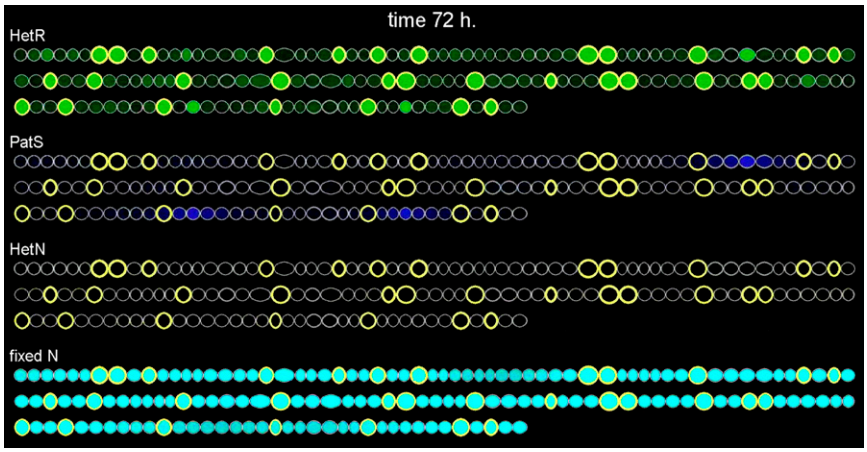

Movie S3. Temporal evolution of gene expression in a filament for *hetN* loss of function. Time counts hours after nitrogen deprivation. Heterocyst cells have a yellow membrane. The intensity of the green, blue, and cyan colors show the level of HetR, PatS, and fixed-nitrogen products concentrations, respectively. In the third line, cells are black because they do not express HetN. When a filament is too long to fit in the width of the movie, it is continued in a row below. The last cell on the right of a row is a neighbor of the first cell on the left of the row immediately below.

Movie S3

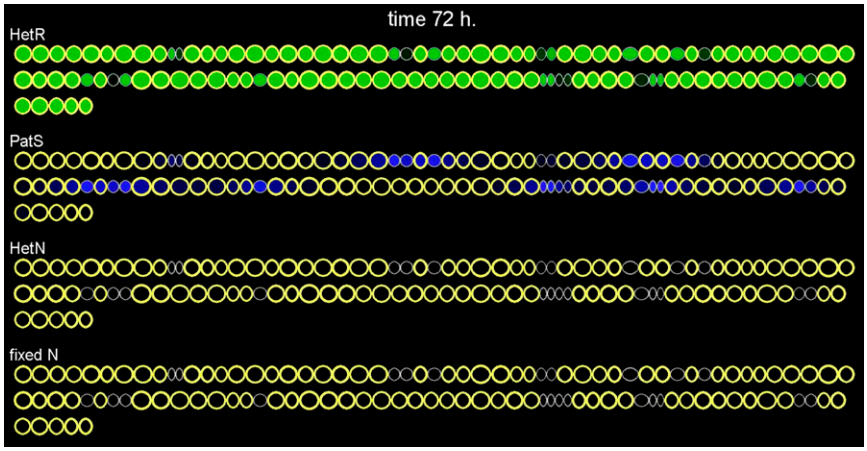

Movie S4. Temporal evolution of gene expression in a filament for *hetN* and fixed-nitrogen loss of function. Time counts hours after nitrogen deprivation. Heterocyst cells have a yellow membrane. The intensity of the green and blue colors show the level of HetR and PatS concentrations, respectively. In the third and fourth lines, cells are black because they do not produce HetN or fixed-nitrogen products. When a filament is too long to fit in the width of the movie, it is continued in a row below. The last cell on the right of a row is a neighbor of the first cell on the left of the row immediately below.

Movie S4

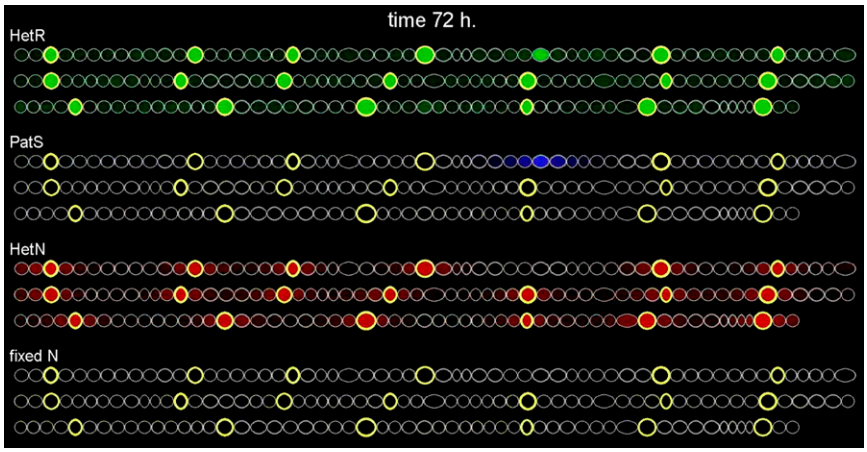

Movie S5. Temporal evolution of gene expression in a filament for fixed-nitrogen loss of function. Time counts hours after nitrogen deprivation. Heterocyst cells have a yellow membrane. The intensity of the green, blue, and red colors show the level of HetR, PatS, and HetN concentrations, respectively. In the fourth line, cells are black because in this condition fixed-nitrogen products have no function in heterocyst differentiation. When a filament is too long to fit in the width of the movie, it is continued in a row below. The last cell on the right of a row is a neighbor of the first cell on the left of the row immediately below.

Movie S5